A CMOS Amperometric System for Multi-Neurotransmitter Detection

Genevieve Massicotte, Sandro Carrara, *Senior Member, IEEE*, Giovanni Di Micheli, *Fellow, IEEE*, and Mohamad Sawan, *Fellow, IEEE*

***Abstract*—*In vivo* multi-target and selective concentration monitoring of neurotransmitters can help to unravel the brain chemical complex signaling interplay. This paper presents a dedicated integrated potentiostat transducer circuit and its selective electrode interface. A custom 2-electrode time-based potentiostat circuit was fabricated with 0.13 μm CMOS technology and provides a wide dynamic input current range of 20 pA to 600 nA with 56 μW, for a minimum sampling frequency of 1.25 kHz. A multi-working electrode chip is functionalized with carbon nanotubes (CNT)-based chemical coatings that offer high sensitivity and selectivity towards electroactive dopamine and non-electroactive glutamate. The prototype was experimentally tested with different concentrations levels of both neurotransmitter types, and results were similar to measurements with a commercially available potentiostat. This paper validates the functionality of the proposed biosensor, and demonstrates its potential for the selective detection of a large number of neurochemicals.**

***Index Terms*—Amperometric readout, CMOS potentisotat, electrochemical biosensor, electrode functionalization, neurotransmitters detection.**

I. Introduction

MONITORING of multiple biological analytes in real-time is highly valuable to increase knowledge on humans complex biological processes and their malfunctions, paving the way to new detection methods and cures for diseases. In the case of brain chemical signaling interplay, precise *in vivo* detection and quantification of multiple neurotransmitters would provide important insights on the brain functioning and its neurodegenerative diseases, by enabling correlation between neurotransmitters concentration fluctuations and specific behaviors. For example, dopamine and glutamate monitoring could explain their role in psychiatric disorders such as Schizophrenia, leading to effective treatments [1]. Current state-of-the-art *in vivo* laboratory techniques include voltammetry and microdialysis with external benchtop equipments for the brain fluid sample analysis [2]–[4]. However, these techniques involve the use of large measuring electrodes, disturbing the cerebral environment, in addition to their inability to be chronically implanted which restricts the possible length of studies [4].

Recently, miniaturized electrochemical biosensors with CMOS technology have been widely used to characterize the concentrations of a variety of biological compounds such as proteins and DNA [5]–[8]. Generally speaking, an electrochemical sensor consists of a transducer coupled with measuring electrodes, that interacts with molecules or the probed solution, creating a charge-transfer reaction that is further converted into an equivalent electrical signal and digitized. These microsystems provides a low-cost and fully integrated solution to multi-analyte monitoring with simple measurement processing, and the possibility of using a large variety of compatible post-fabrication processes to develop selective and sensitive interfaces. Also, total integration of the electrode interface with the required transducer electronics can improve the measurement accuracy by reducing the effects of external noise.

Few works have proposed CMOS electrochemical biosensors for neurotransmitters sensing, using ISFETs [9], capacitive detection [10], [11], or amperometry/voltammetry techniques [12]–[14]. The latter transduction mechanism is the most performing in a highly conductive medium [15], such as the brain extracellular liquid [16]. However, existing biosensor devices using amperometry/voltammetry [12]–[14] are conceived for *in vitro* applications and are often limited to a single target detection without considering the complexity of *in vivo* environment which raises selectivity and sensitivity issues. Indeed, more than one hundred types of neurotransmitters evolve in the brain extracellular liquid, which is a highly complex molecular medium [16], meaning that a selective sensor is needed to unequivocally detect specific molecules. Also, sensitivity diminishes when using miniaturized interfaces such as microelectrodes, since the measuring area decreases, decreasing the signal to noise ratio, and consequently the concentration range measured. Moreover, current biological findings states that the minimum concentration time variation of neurochemicals is a couple of milliseconds [17], demanding a sensor with a minimum sampling frequency of 1 kHz for real-time analysis. Finally, a system with a large input dynamic range is needed to detect a variety of neurotransmitter physiological concentration range. The overall valuable concentration range is estimated to vary between nM and mM [2], [18] which approximately

Manuscript received June 08, 2014; revised January 21, 2015 and August 20, 2015; accepted September 01, 2015. Date of publication January 08, 2016; date of current version March 04, 2016. This paper was supported by NSERC, Canada Research Chair on Smart Medical Devices, UE project ERC-2009-AdG-246810. This paper was recommended by Associate Editor R. Genov.

G. Massicotte and M. Sawan are with Department of Electrical Engineering, Polystim Neurotechnologies Laboratory, Ecole Polytechnique Montreal, Montreal, QC H3C 3A7, Canada (e-mail: genevieve.massicotte@polymtl.ca; mohamad.sawan@polymtl.ca).

S. Carrara and G. Di Micheli are with Integrated Systems Laboratory, Ecole Polytechnique Federale Lausanne, 1015 Lausanne, Switzerland (e-mail: sandro.carrara@epfl.ch; giovanni.demicheli@epfl.ch).

Color versions of one or more of the figures in this paper are available online at http://ieeexplore.ieee.org.

Digital Object Identifier 10.1109/TBCAS.2015.2490225

translates into current levels ranging from 1 pA to 1 μA, using Cottrell equation [15]. The system sensitivity to a certain neurotransmitter depends greatly on the electrode coating used, which vary greatly by their composition. A large dynamic range is required to accommodate all sort of electrode, reducing the limitation put on their selection.

In order to meet these specifications, we propose in this work a multi-target amperometric biosensor performing constant-voltage amperometry (CA). CA and fast-scan voltammetry (FSCV) are the two most commonly used electrochemical methods for neurotransmitters characterization. FSCV provides a high selectivity at the expense of a temporal resolution in the order of 100 ms and a more complex implementation and result processing than CA. The chemical sensitivity of this method is considered lower than CA, which resolves in the addition of chemical coatings on the measuring electrode surface to increase the sensitivity [20]. CA has low selectivity, but is the fastest electrochemical technique available, limited only by the signal to noise ratio and the sampling frequency [19]. The use of chemical coatings on the electrode surface coupled to CA can provide high selectivity toward specific targets, as well as enhanced sensitivity. Also, only a potentiostat in a simple configuration is required as the transducer. Such potentiostat is an electronic circuit that maintains a constant-voltage difference between a reference electrode (RE) and a working electrode (WE), producing an electrochemical or *redox* reaction between an electroactive species of interest and WE. The electron transfer resulting from that reaction produces either an oxidation current or a reduction current. Oxidation is the loss of electrons at the electrode, while reduction current implies the gain of electrons. This current is directly proportional to the species concentration, and measured by the potentiostat. A variety of 2-electrode integrated potentiostat circuit architecture have been proposed these past years for low current detection, involving current conversion into digital pulses using sigma-delta modulators [21]–[23] or comparators [24], [25]. However, the trade-off between the sampling frequency, low-power consumption and wide dynamic range needed by our application and achieved by these designs can still be improved. Therefore, a new CMOS potentiostat circuit architecture optimized for this application is proposed in this work. On the other hand, a multi-target interface for amperometry measurements requires a multi-WE sensing platform. To provide enhanced sensitivity and selective measurements, we propose to functionalize each WE with specific carbon nanotubes (CNT) based chemical coatings. CNT have shown to increase sensitivity and electron transfer kinetics by several works [26]. Furthermore, they provide suitable properties for biosensing, such as chemical stability, mechanical strength, high electrical conductivity [27], [28], and biocompatibility according to recent studies [29]. This nanomaterial, coupled with specific molecules such as polymers and enzymes, creates discrimination between the interactions without degrading the molecules active properties, as well as providing a strong immobilization method [30]. Most published work involving simultaneous detection of neurotransmitters are limited to the design of the electrode chemical coating [31]–[33], which are tested with benchtop laboratory equipment, and dont imply

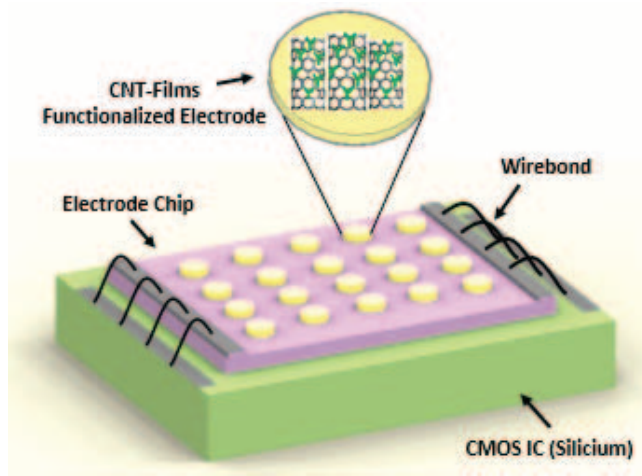

Fig. 1. Long-term targeted fully-integrated amperometric biosensor architecture.

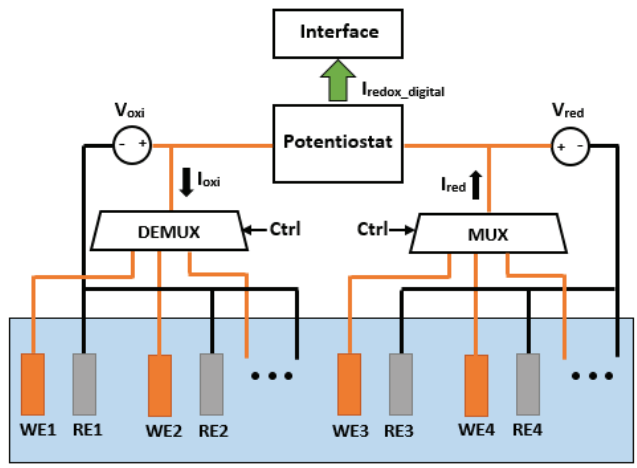

Fig. 2. Detection circuit architecture.

the proposition of a fully integrated biosensor system. To our knowledge, a comparable implantable system designed to provide long-term multi-neurotransmitters concentration measurements in the brain has not been reported.

Toward a fully-integrated microsystem, this paper concerns a proof-of-concept of such sensor, with the experimental validation of a CMOS integrated transducer and a multi-WE selective sensor interface, using different concentration levels of glutamate and dopamine. This paper is organized as follows. Section II presents the system architecture considered as long-term development. Section III describes the CMOS potentiostat IC electronic architecture and operation principle. Section III presents the multi-WE sensor interface architecture and functionalization. In Section IV, experimental results regarding the fabricated potentiostat circuit characterization are first described, followed by biological measurements conducted with the sensor prototype.

II. System Architecture

Fig. 1 illustrates the conceptual biosensor system architecture for *in vivo* neurotransmitters detection that represents the vision guiding the development presented in this paper. The electronic

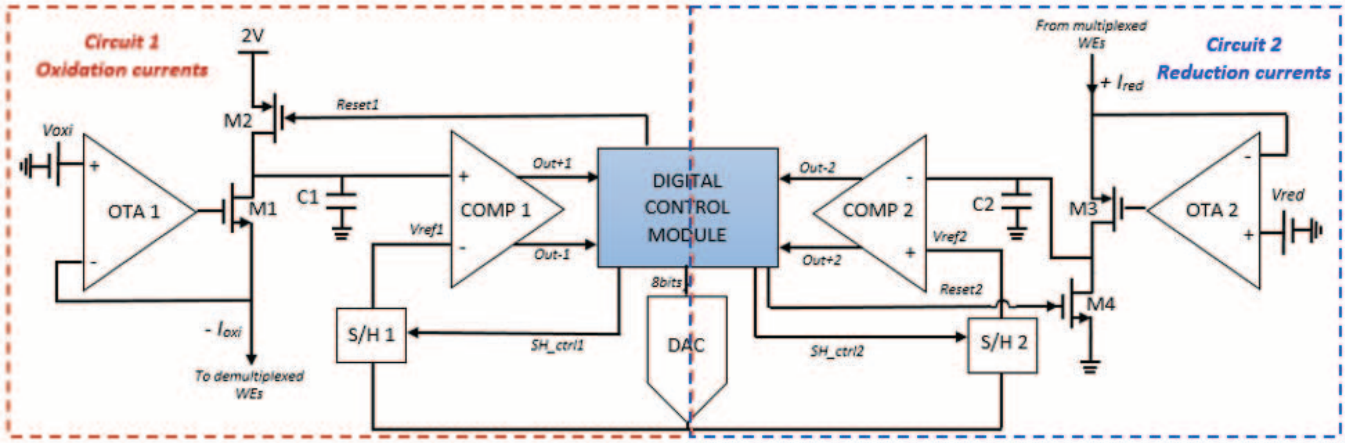

Fig. 3. Top-level time-based potentiostat circuit for oxidation currents (circuit 1) and reduction currents (circuit 2) measurements.

circuits, such as the potentiostat transducer, data transmission and power management modules are fabricated with CMOS technology on a silicon chip. The multi-WE functionalized sensing interface chip is placed on top and is connected to the potentiostat circuits using wire-bounding. Furthermore, the integration of the sensing electrodes directly on the CMOS chip is also a possibility. CMOS technology can offer a fully integrated system, with the advantage of low-production costs. Such integration will be done to connect on chip the electrode arrays to built in transducer, limiting the measurement noise. Although, post-processing is required since CMOS technology offers a limited selection of materials. In addition, the transducer circuits must be sealed from the electrodes array, which also demands complex post-processing steps. A biocompatible encapsulation packaging could also be used to protect the circuits and connections from the biological liquids, while leaving the electrode interface indirect contact with the biological fluids. Fig. 2 illustrates the general detection circuit architecture considered involving the potentiostat transducer and multi-WE platform for multiple target quantification. Each WE, associated with the detection of a single neurotransmitter type, is connected sequentially to the potentiostat input by the control of a multiplexer/demultiplexer (mux/demux). *Redox* bias voltages (Voxi/Vred) are provided by an external voltage generator and modified to correspond with the measured neurochemical. RE of each channel are connected to the same fixed potential, simplifying the circuitry required. We consider the use of a 2-electrode potentiostat instead of the common 3-electrode configuration since the current density of our application is considered low ($<100\ \mu$A/cm^2), thus only a negligible polarization of RE might occur [15]. Moreover, the 2-electrode configuration also implies a simpler implementation, reducing space and power consumption.

III. CMOS Potentiostat IC

Fig. 3 illustrates the time-based potentiostat circuit proposed. This circuit measures oxydation and reduction currents separetly using symetrical circuits, respectively circuits 1 and 2. Digitized time measurements directly proportional to the *redox* current levels at WE are obtained without any complex analog to digital conversion circuit, adding a quantification error to the measurement. The circuit is designed with IBM 0.13 μm CMOS technology.

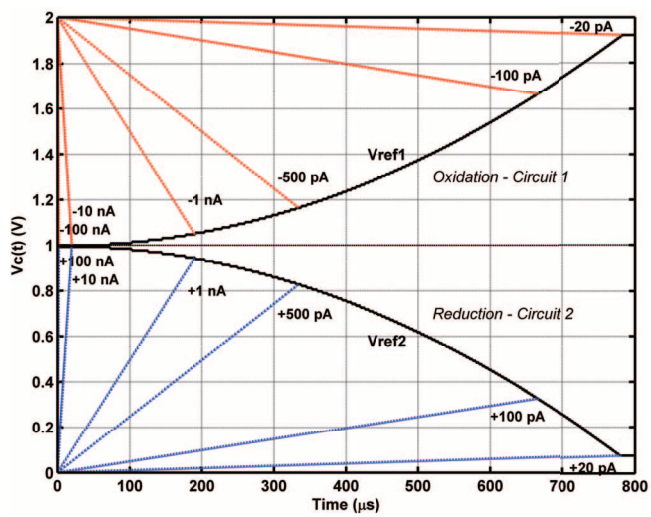

Fig. 4. Different output voltages across $\mathrm{C}(V_c(t))$, versus time measurement for different magnitudes of oxidation (red traces) and reduction currents (blue traces), with V_{ref} varying according to a quadratic function of time.

A. Operation Principle

The circuit operation principle relies on the discharging (oxydation currents) or charging (reduction currents) of a measuring capacitor C to a threshold voltage level V_{ref}. The time taken to reach V_{ref} is directly proportional to the *redox* current at WE by the following equation:

$$\frac{\Delta V_c}{\Delta t} = \frac{V_{\mathrm{ref}}(t_f) - V_c(t_0)}{t_f - t_0} = \pm \frac{i}{C}. \tag{1}$$

V_{ref} is varied according to a quadratic function of time, in order to optimize the sampling frequency. Thus, the maximum time measurement corresponding to the lowest *redox* current detected is decreased, which increases the sampling frequency. Fig. 4 illustrates this concept, with different plotted capacitor output voltages versus time measurement, for various oxidation and reduction currents. According to (1), using a C of 200 fF

value, *redox* currents ranging from 20 pA to 800 nA can be detected at a frequency of 1.25 kHz, with C output voltage (Vc) varying between 0.125 V and 1 V. Each circuit is made of a current conveyor stage (OTA, M1/M3, M2/M4), a comparator, and a shared digital-to-analog converter (DAC). In circuit 1, C_1 is pre-charged at 2 V by a reset signal (Reset1) applied to PMOS transistor M2, at the sampling frequency. The oxydation current discharges C_1 through M1 that acts as a buffer. The comparator compares continuously the voltage across C_1 to $V_{\rm ref}$ adaptative value, which is generated by the DAC. When these voltages crosses, a pulse is generated at COMP positive output (Out+1). The digital control module (DCM) detects the logic level change with a falling edge detector, and counts the delay between pulses which translates into time measurements. These time measurements are converted into concentration levels using the calibration curve associated with the sensed neurotransmitter. The same operation principle applies for reduction currents measurements with circuit 2, except that the operation is reversed, as C_2 is charged through M3 over time. M4 NMOS reset transistor grounds C_2 before each new measurement. The main advantage of the proposed potentiostat topology compared to a conventional structure involving a CTIA front-stage converting the input current into a voltage level followed by an ADC for digitization, is the fast conversion rate achieved for a wide range of input current. Indeed, the comparator paired with the DAC operates a single-slope ADC and allows a high sampling rate for currents ranging from few pA to hundreds of nA. Although, the current conveyor input stage offers a lower input noise immunity compared to a CTIA one, sub-level pA resolution can still be achieved by sizing properly its components transistors. Moreover, in the case of CA, only a reduction or an oxidation reaction can occur at the electrode. This potentiostat architecture allows to detect these two current types separately, and therefore use a time-based topology using half of the circuit required for CV or FSCV electrochemical techniques.

1) Current Conveyor: The current conveyor maintains the OTA negative input constant at the voltage that biais WE (V_{oxi}/V_{red}), and isolate the input *redox* current signal from the measuring capacitor C by using a cascode transistor that acts as a buffer. In fact, this circuit provides a low input impedance in order to achieve a high *redox* current injection ratio and a high output impedance to avoid any disturbance at the OTA negative output. A two-stage folded cascode-Miller OTA, illustrated on Fig. 5, was designed to provide low input noise, wide output voltage swing, low power and high gain. Indeed, a high gain is required to obtain high output impedance and low input impedance. A rail-to-rail output swing is reached by adding the second stage, necessary to achieve the detection of a wide range of input currents. The critical parameters of the OTA are presented in Table I. Reset transistors M2 and M4 are designed with minimum width and length to reduce charge injection in C. For circuit 1, C is reset to 2 V in order to reduce power consumption of the system. 2 V is chosen as a compromise between lowering the voltage supply of the comparator and DAC, and keeping a viable saturation operation of the cascode transistor M1 for the largest *redox* current range. The OTA M1 and M2 transistors (Fig. 5) are sized with large width and length to induce high transconductance. The current mirror transistors M8 to M11 and the polarization transistors M6/M7 and M17/M18 are sized to operate in saturation mode providing stable sources of current.

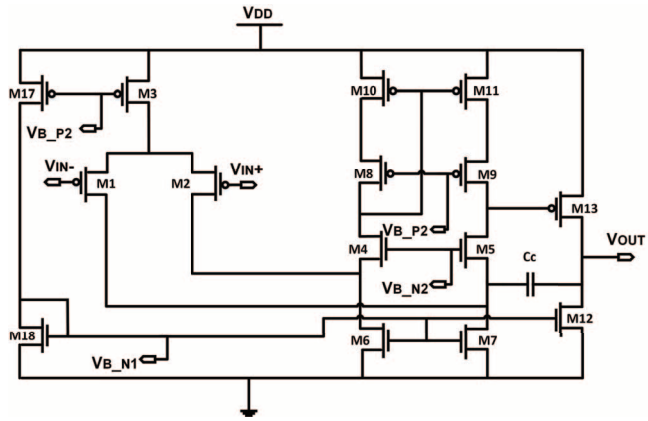

Fig. 5. *Folded cascode-Miller* OTA circuit.

TABLE I
MAIN CIRCUIT PARAMETERS

OTA	
DC Gain	85 dB
Output swing range	0,03–2,43 V
Bandwidth	4 kHz
CMRR	100 dB
Power supply	2,5 V
Power consumption	15 μW
Comparator	
Clock frequency	100 MHz
Delay	1,74 ns
Kickback noise	0,7 mV
Offset voltage	1,2 mV
Power supply	2 V
Power consumption	18,2 μW
DAC	
Latency	230 ns
INL	+/-0.75
DNL	+/-1.01
Offset error	80 mV
Power supply	2 V
Power consumption	39 μW

2) Comparator: The comparator compares continually C output voltage with $V_{\rm ref}$, producing a digital pulse when these values cross, ending the measurement. A 100 MHz comparison speed is needed to measure nanoamps *redox* currents producing nanoseconds time measurements. A class-AB latched comparator, illustrated on Fig. 6 is used for its high speed, low power consumption, rail-to-tail operation, and low offset voltage. This dynamic comparator works in a reset state followed by a decision state at a frequency of 100 MHz. A kickback noise cancellation circuit, proposed by Figueiredo *et al.* [34] is also added, reducing this parasitic effect by 20 times. Kickback noise is caused by large voltage variations on the comparator regeneration nodes which couples the comparators input transistor through their parasitic capacitances. It can strongly alter the time measurements precision produced since it disturbs the input voltage of the comparator and consequently the charge or discharge speed of C. Post-layout simulations characterizing the effectiveness of this kickback noise reduction

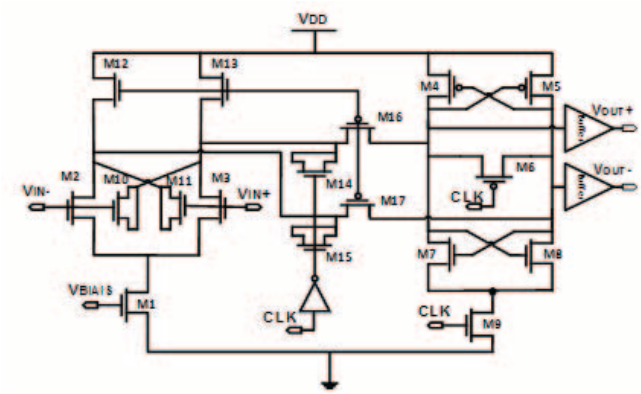

Fig. 6. Class-AB latched with *kickback* reduction comparator circuit.

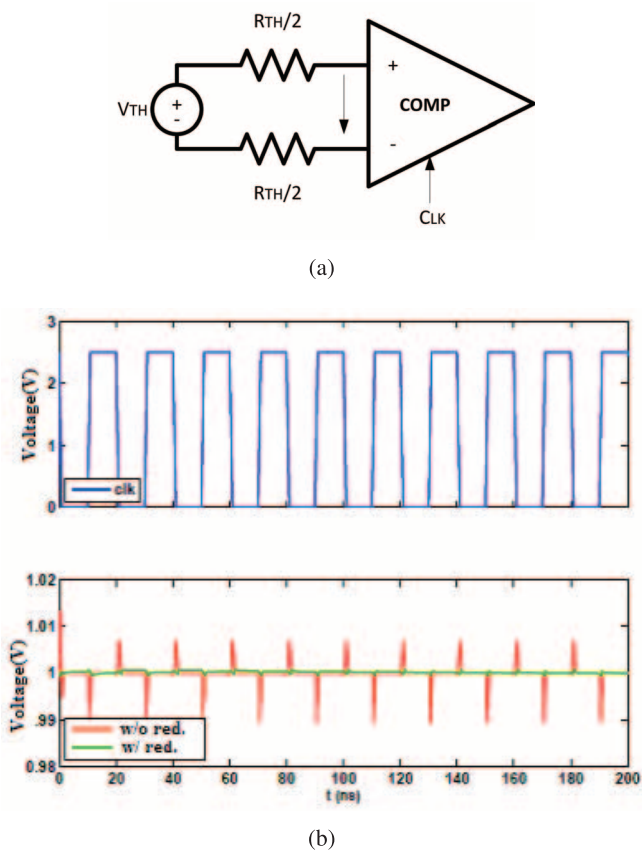

Fig. 7. *Kickback* noise cancellation circuit effectiveness (a) Test circuit. (b) Post-simulation results with and without the circuit.

circuit are shown in (Fig. 7). The stage preceding the input of the comparator is modeled with a Thevenin equivalent circuit with Rth = 8 kW and Vth = 1 V. Kickback noise is reduced over twenty times from 14 mV to 0.7 mV, as shown by the simulation of the input differential voltages in fig 3.12 (b). The critical parameters of the comparator are presented in Table I. Transistors M14 to M17 (Fig. 6) act as loads to the differential pair and are sized so as to maintain the drain voltages of M2/M3 equal to the values obtained during the reset phase. Transistors M10/M11 are sized with minimum length and a half the width of the transistors M2/M3, forming two capacities of equivalent

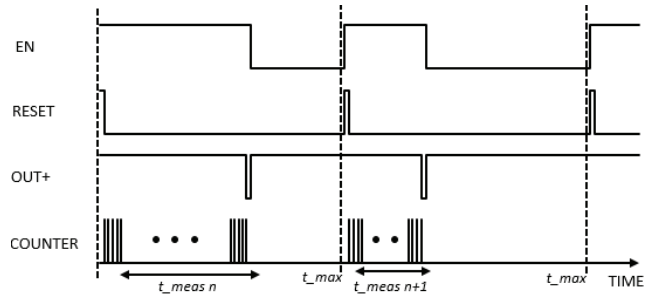

Fig. 8. Sampling digital signals produced by the digital control module.

value to the gate-drain parasitic capacity of the differential pair which have the effect of reducing the kickback noise.

3) DAC: A 8-bit DAC with a current-steering topology adapted from Yi *et al.* [35] is chosen for its high speed and low power consumption. For each 2-bit segment, the input binary code is transfered to a 3 digits thermometer code using logic gates. Each digit controls respectively a current source. A total of 12 current sources are used to create an 8-bit DAC. The critical parameters of the DAC are presented in Table I. Also, sample-and-hold (S/H) circuits filter output glitchs and maintains V_{ref} value during the period requested, allowing to share the DAC between both channels.

4) Digital Control Module: The digital control module is responsible for the modulation of the *Reset*, V_{ref}, SH_{ctrl} and *En* control signals and the sampling of the output signals *Out*. First, *En* is activated, powering up the comparator and the DAC during 3.5 μs. The OTA is always on to assure the continuity of the electrochemical reaction ongoing. Each measurement starts when the *Reset* signal is disabled. The counter signal $t_{counter}$ is reset to 0 and V_{ref} is set to its first value. V_{ref} is pre-programmed and varied iteratively in function of $t_{counter}$. V_{ref} 8 bits discretization for the sampling time period is generated to the DAC using a digital circuitry implemented in the FPGA with VHDL description language. This digital circuitry consists of an adder, comparators and a 256 byte ROM memory containing the discretized time values for each 8-bit combination. When the measurement ends, the time measurement (t_{meas}) equals $t_{counter}$ and *En* signal is disabled. When $t_{counter}$ reaches the maximum time $(t_{\max})$ value fixed by the sampling period, the process is repeated. Fig. 8 summarizes the digital signals sampling algorithm.

B. Limitation Analysis and Circuit Optimization

Several factors can undermined the proposed potentiostat performances by affecting the measurement resolution and input range. A theoretical analysis of the relative measurement error and a noise analysis are made in order to optimize the circuit components consequently.

1) Relative Measurement Error: The current measurement relative error depends on the comparator and DAC precision, and V_{ref} function form. From (1), this parameter is expressed by the following equations:

$$\frac{\Delta i}{i} = \frac{\left(\left|\frac{\partial i}{\partial t}\right|\Delta t + \left|\frac{\partial i}{\partial V_{\mathrm{ref}}}\right|\Delta V_{\mathrm{ref}}\right)}{i} \tag{2}$$

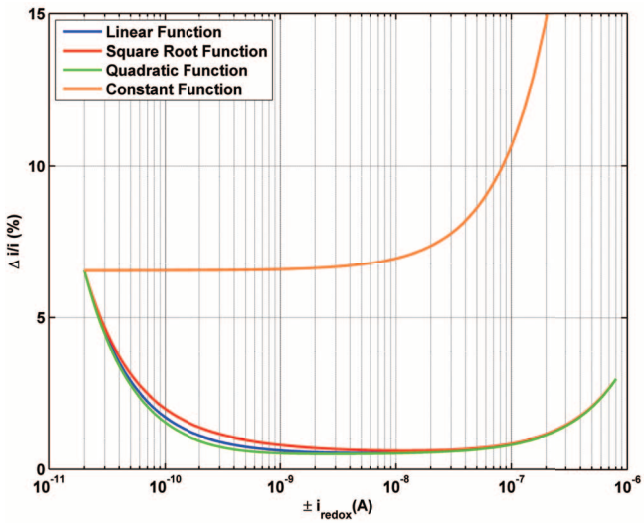

Fig. 9. Relative error measurement for four different $V_{\rm ref}$ types.

$$\frac{\Delta i}{i} = \frac{\left(\frac{C(V_c t_0 - V_{\rm ref})}{t^2}\Delta t + \frac{C}{t}\Delta V_{\rm ref}\right)}{i} \tag{3}$$

where $\Delta V_{\rm ref}$ is the DAC precision and Δt is the measurement precision that depends on the dynamic comparator precision, described by the following equation:

$$\Delta t = \frac{CV_{\rm off}}{i} + t_{del} + t_{pclk/2} \tag{4}$$

where $V_{\rm off}$ is the comparator's offset voltage, t_{del} is the response delay and $t_{pclk/2}$ the half period of the clock, counting the time the comparator is in *Reset* mode. Considering (2)–(4), $V_{\rm ref}$ function type influences the relative measurement error since for a given input current, the error decreases the larger the associated time measurement is. Fig. 9 shows the theoretical relative error current measurements as a function of the input current for four different $V_{\rm ref}$ functions of time passing at points (1 V, 1 μs) and (1.925 V, 750 μs): constant function at 1.925 V, linear function, quadratic function and a squared root function. A maximum error value of 38% is calculated for the constant function, and 6.65% for the other three. The quadratic function shows the lowest cumulative error value on the entire input current range concerned, and is therefore implemented in the presented work.

2) Noise Analysis: The input referred noise at a single WE ($\overline{In_{eq}{}^2}$) limits the minimum current value detected by the potentiostat. This parameter depends on the front-end noise sources, including the OTA, the buffer transistor M1 (In_{M1}) and the noise generated by the electrochemical reaction and electrodes (In_{rx}). The noise generated by the multiplexer and the OTA second stage are considered negligible. $\overline{In_{eq}{}^2}$, including thermal (th) and flicker ($1/f$) noise components, is given by the following equation:

$$\overline{In_{eq}{}^2} = \overline{In_{M1}{}^2} + \overline{gm_{M1}{}^2 Vn_{OTA}{}^2} + \overline{In_{rx}{}^2} \tag{5}$$

with

$$\begin{aligned}\overline{Vn_{OTA}{}^2} = &\left(\frac{2K_n}{C_{ox}W_{M6}L_{M6}f}\left(\frac{gm_{M6}}{gm_{M1}}\right)\right.\\ &+\frac{2K_p}{C_{ox}W_{10}L_{10}f}\left(\frac{gm_{M10}}{gm_{M1}}\right)\\ &\left.+\frac{2K_p}{C_{ox}W_{M1}L_{M1}f}\right)_{1/f}\\ &+\left(\frac{4kT}{gm_{M1}}\left(\frac{4}{3}\right)\left(1+\frac{gm_{M6}}{gm_{M1}}+\frac{gm_{M10}}{gm_{M1}}\right)\right)_{th}\end{aligned} \tag{6}$$

where, gm_M, f, k, T, C_{ox}, K, and γ, are respectively, the transconductance of transistor M, the frequency, the Boltzmann constant, the temperature, the gate oxide capacitance, the flicker noise constant of transistor type, and the transistor factor. The cascode transistor is operated in subthreshold during picoamps current level detection. Therefore, In_{M1} is given by [36]

$$\overline{Vn_{M1}{}^2} = \left(\frac{4kT_K}{W_{M1}L_{M1}f}\right)_{1/f} + \left(\frac{2qI_{WE}}{gm^2}\right)_{th} \tag{7}$$

where, q and I_{WE}, are respectively, the electron charge and the current at WE. Similarly, $\overline{In_{eq}{}^2}$ can be found for circuit 2 by replacing M1 by M3 (Fig. 3) in (5). Considering (5)–(6), in order to minimize the OTA noise, $gm_{M6,7}$ and $gm_{M10,11}$ must be $\ll gm_{M1,2}$. This has been done by biasing the OTA input differential pair (M1,2) in the subthreshold region with large size, where the transconductance efficiency gm/Id is enhanced, and biasing active load transistors (M6,7 and M10,11) in the saturation region to minimize their gm and assure a stable response. A compromise between obtaining a low noise level and a high output impedance is achieved by sizing the cascode transistor with a large length and a narrow width. The simulated input-referred current noise of the circuit front-end is 0.013 pA/$\sqrt{\rm Hz}$ for a bandwidth of 1 kHz, offering suitable noise performances for sub-pA resolution.

IV. Multi-WE Platform

A multi-WE platform acting as the biosensor interface is fabricated with microfabrication processes. Each WE is functionalized with CNT based composite films to assure a selective and sensitive detection towards both glutamate and dopamine. Dopamine is directly detected, while glutamate is indirectly detected with the use of Glutamate Dehydrogenase (GLDH) enzyme that produces electroactive Nicotinamide Adenine Dinucleotide (NADH).

A. Architecture

The electrode chip is composed of 5 gold WEs, allowing the detection of up to five different analyte depending of their functionalization. Each WE have an area of 0.25 mm^2. A common platinum RE and a gold counter electrode (CE) are also present. The CE is necessary to validate the chip functionality with a commercial laboratory potentiostat, although it is not used in

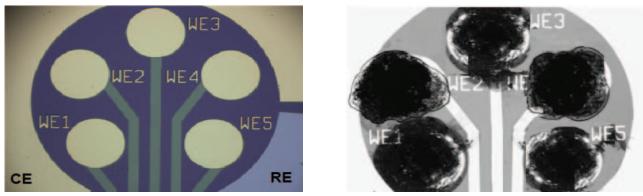

(a) (b)

Fig. 10. Chip with multiple gold WE, a common platinum RE and gold CE. (a) Unspotted. (b) Spotted with CNT-based films: Nafion-MWCNT on WE1-W3-W5 and MDB-CHIT-MWCNT-GIDH on WE2-WE4.

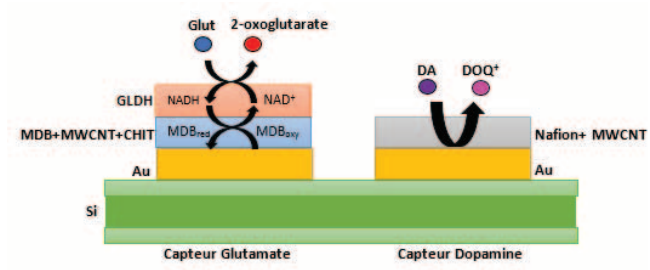

Fig. 11. Schematic of the CNT-based films composition of the glutamate and dopamine sensor, and the respective oxidation reaction occurring at the gold (Au) electrode interface.

the proposed biosensor system. The chip is fabricated on a silicon substrate using the same processing steps has described in a previous work [37].

B. Electrode Functionalization

Both films are made from Multi-Walled CNT (MWCNT) has they provide a high electrochemical stability [26]. MWCNT (diameter 10 nm, length 1–2 μm) in powder form (95% purity), purchased from DropSens (Spain) are used. All other chemical products were purchased from Sigma-Aldrich and were used has received. All solutions were prepared using Millipore water.

1) Dopamine Sensor: A Nafion-based MWCNT solution is used to exclude anions, such as ascorbic acid and uric acid, which can interfere with dopamine detection since they share a similar *redox* potential. Nafion is also used for its high solubility [38], which facilitates the CNT deposition with the spotting method used. MWCNTs are dispersed at a concentration of 1 mg/ml in a solution of Millipore water 50 vv% and ethanol 50 vv%, with 0.5 wt% Nafion.

2) Glutamate Sensor: A composite film made from MWCNT, chitosan (CHIT), meldola's blue (MDB), and GLDH enzyme is used to selectively detect glutamate with a high sensitivity [39]. MDB is a *redox* mediator that increases the reaction response time and lowers the oxidation peak level (-200 mV). The latter effect discriminate glutamate detection from dopamine which is associated to a higher peak potential. MWCNT are dispersed at a concentration of 100 mg/ml in a solution of CHIT (0.05 % in 0.05 M HCL) at 98.4 vv% and MDB (5 mM ethanolic solution) at 1.6 vv%.

The fabricated chip un-functionalized and functionalized is shown on Fig. 10. Fig. 11 summarizes the films composition used for the detection of both compounds, and the respective *redox* reactions occurring. CNT-based composite films are drop-casted on each WE using an automatic spotting machine commercially available (Sci-Flexarrayer DW by Scienon, Germany) [37]. 800 nL of Nafion-MWCNT solution is deposited on each of the following: WE1, WE3, and WE5. 200 nL of MDB-CHIT-MWCNT solution is spotted on WE2, and WE4, followed by the deposition of 400 nL of GLDH enzyme on each electrode.

V. Experimental Results

Before testing the biosensor system, the accuracy and precision of the fabricated integrated potentiostat, as well as the sensitivity and selectivity of the multi-WE platform, were individually characterized. Afterwards, the complete system was tested

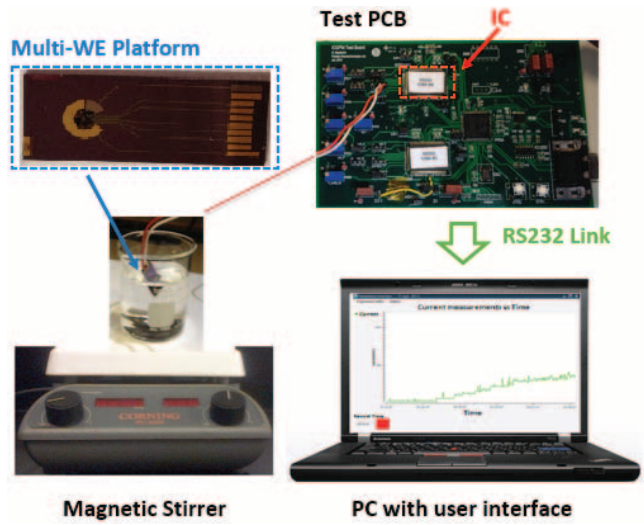

Fig. 12. Experimental test setup for the proposed biosensor system.

with biological solutions of dopamine and glutamate. Fig. 12 summarizes the test setup used for the resulting multi-neurotransmitter biosensor system. The fabricated potentiostat IC is mounted on a printed circuit board (PCB) that includes a FPGA acting as the digital control module for control signals generation and data acquisition. An RS-232 link is implemented in the FPGA to allow data transmission of the potentiostat time measurements on a computer in real-time. The PCB is designed with signal integrity methods such as digital and analog plane separation and signal shielding. The functionnalized multi-WE platform is connected to the IC input through wires and a low injection noise analog multiplexer, and dipped in a beaker containing the neurochemicals. A user interface realized with *Qt* software records and plots the resulting amperometric measurements made by the integrated potentiostat.

A. Potentiostat Characterization

The potentiostat IC layout and micrograph are shown on Fig. 13. A printed circuit board (PCB) including an FPGA was developed to characterize efficiently the potentiost IC. An RS-232 link is implemented in the FPGA to obtain the produced time measurements on a computer user interface in real-time. An external current source (Keithley 236) is used at the IC input, simulating the different *redox* currents from picoamp to microamp levels, normally generated by electrochemical reactions involving neurotransmitters. Currents ranging from

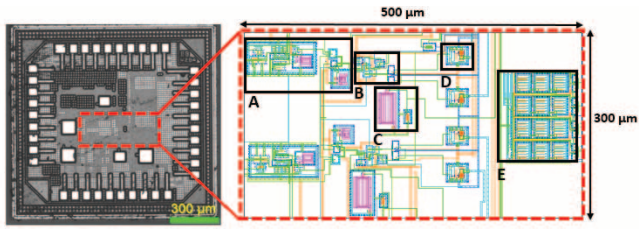

Fig. 13. IC micrograph and layout view of the CMOS potentiostat with (a) current conveyor stage, (b) comparator, (c) S/H circuit, (d) output test buffer, and (e) 8-bit DAC.

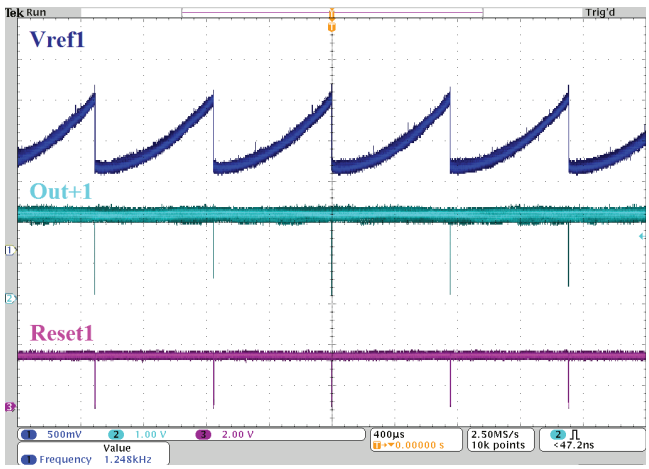

(a)

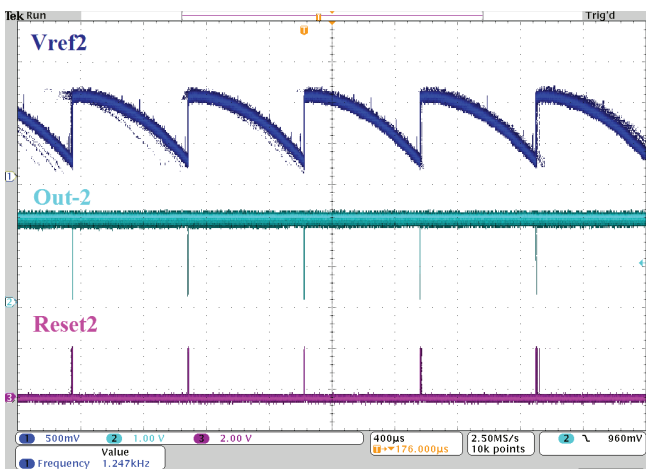

(b)

Fig. 14. Potentiostat IC critical generated waveform collected at the oscilloscope for a *redox* current measurement of 20 pA at a frequency of 1.25 kHz. Individual measurement of (a) −20 pA and (b) 20 pA. Successive measurement of (c) −20 pA and (d) 20 pA. From top to bottom: V_{ref} (0,5 V/div), *Out* (1 V/div) and *Reset* (2 V/div).

20 pA to 600 nA can be detected at a minimum frequency of 1.25 kHz. Fig. 14 shows the typical signals generated by the potentiostat, collected from the oscilloscope (Tektronix MD04104-6) for the measurement of a 20 pA *redox* current at a frequency of 1.25 kHz. V_{ref}, *Out*, and *Reset* signals are presented. C output voltage signal was not probed due to the high parasitic capacitance associated with the oscilloscope probes and chip pads (pF range) compared to C value (fF range). The measured conversion curve of time measurements and current input are presented in Fig. 15(a) for oxydation and reduction currents. Fig. 15(b) shows the corresponding current measurements calculated from the time measurements made via (1), considering the variation of V_{ref} as a quadratic function of time. Other than the DAC and comparator precision errors discussed previously, the difference between the theoretical and experimental current measurement is also explained by process variations concerning the fabrication of capacitor C and the injected parasitic charges into it. These charges come mainly from the kickback noise generated by the comparator, as well as the switching reset transistor (M1/M3). These have the effect of charging the capacitor C_1 associated with the measurement of oxidation currents and discharging C_2 associated with the measurement of reduction currents in excess, respectively, producing measurement time higher and lower than theoretical value. Since this phenomenon is linear throughout the current range, a simple calibration step by adjusting the value of capacitor C upwards or downwards in (1) may be performed during the conversion of time measurements into current measurements. The relative measurement error varies from 0,54% to 10% according to the waveform associated to a quadratic function of V_{ref} described on Fig. 9, resulting in a current sensitivity ranging from 1.8 pA to 60 nA.

B. Biological Metabolites Measurements

First the functionalized WEs are characterized using a commercial benchtop potentiostat (AutoLab PGSTAT128N by Methrohm) to validate their sensitivity and selectivity towards dopamine and glutamate. CA analysis are conducted for each functionalized WE using different concentration levels of each neurotransmitter. The same process is repeated with the proposed biosensor system, by connecting the electrode chip to the potentiostat IC.

The multi-WE platform is submerged in a beaker containing 10 ml of Phosphate Buffer Solution (PBS-10 mM, pH 7.4) and 4 mM of NAD+, stirred vigorously at 90 rpm with a magnetic stirrer at room temperature. WE are digitally selected with the multiplexer control signal. A DC potential of +400 mV corresponding to the oxidation peak of dopamine is applied at the potentiostat input for dopamine detection, and −200 mV for glutamate detection. Electrode stabilization was achieved using a blank solution before the beginning of each CA analysis. Also, the platform was kept at a temperature of 4°C to ensure enzyme stability. The amperometric response of WE1, WE3, and WE5 towards dopamine is measured individually, using dopamine concentration injections varying from 0 to 10 μm, with 1 μm steps. This produces a CA curve, such as Fig. 16(a), which depicts a typical CA curve for a dopamine sensor, recorded with the fabricated integrated potentiostat. The time-step between injections depends on current stabilization. The same process is conducted with WE2 and WE4 for glutamate concentrations levels ranging from 0 to 1 mM, with steps of 200 μm. In both cases, the concentration steps were limited by the noise level generated by the experimental setup, especially caused by the magnetic bar rotation in the beaker. Fig. 16(b) and (c) show the average calibration curves obtained with the proposed biosensor system and the commercial benchtop potentiostat, respectively for dopamine and glutamate. An average electrode sensitivity

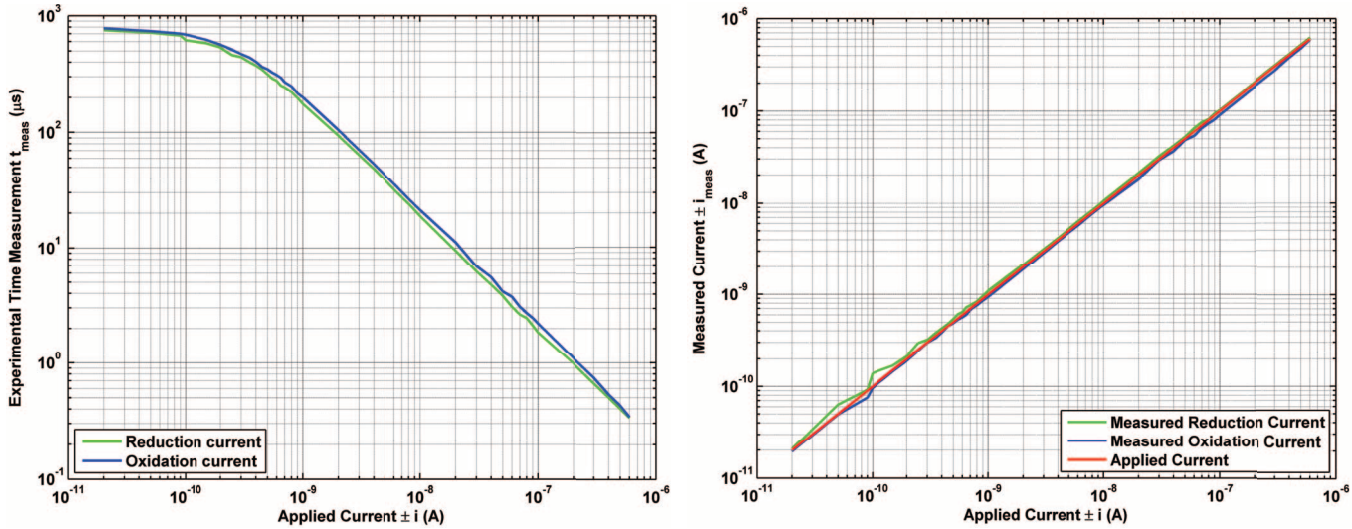

(a) (b)

Fig. 15. (a) Experimental time measurements and (b) calculated experimental current measurements in function of applied current at the circuit input.

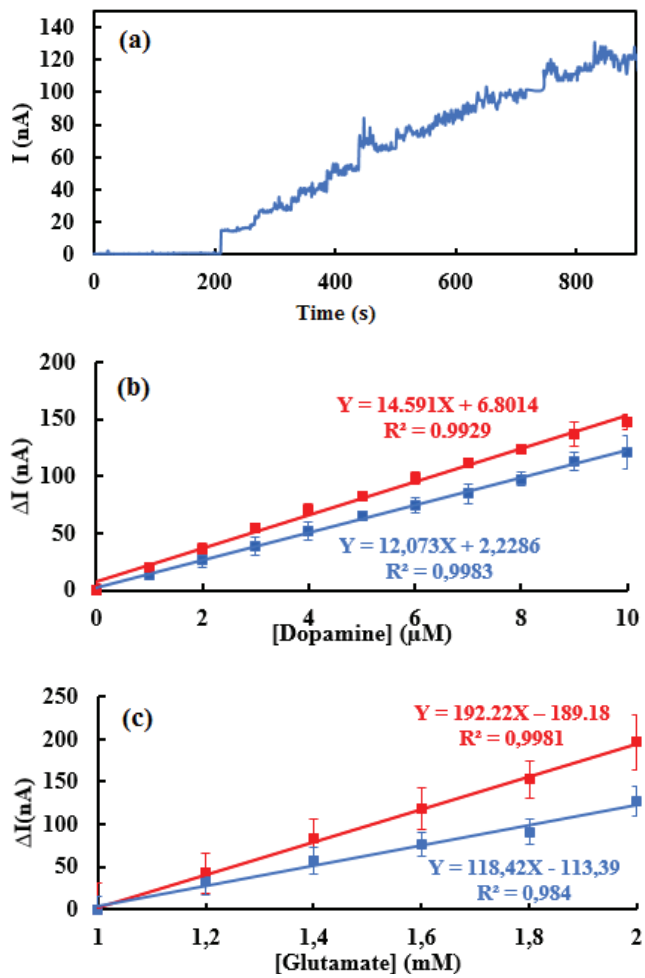

Fig. 16. (a) Typical experimental amperometric current time curve of dopamine sensor, and comparison of calibration curves obtained for (b) dopamine and (c) glutamate detection with the fabricated integrated potentiostat (blue) and the commercial potentiostat (red).

of 12.07 ± 1.48 nA/μm and 118.42 ± 9.10 nA/mM is obtained respectively toward dopamine and glutamate for the measured concentration range. In both cases, a high linearity, characterized by the coefficient of regression $(R2)$ of the linear regression is achieved. The calibration curves are plotted according to the time-current curve resulting from the CA analysis data Fig. 16(a)]. The electrode sensitivity is computed from the calibration curve slope in the linear response range. The sensitivities and linearity measured are similar with the use of the commercial instrument and our circuit, validating the concept of the proposed biosensor system. The response of the two sensors (dopamine and glutamate) in the presence of the interfering substance has been characterized. Fig. 17 shows the response of a dopamine sensor upon the successive injection of **6** μ**M** dopamine steps, followed by glutamate injection steps of 0.1 mM and 1 mM. The same experiment was conducted with a dedicated sensor to glutamate (Fig. 16), by injecting 1.5 mM of glutamate, followed by an injection of 0.1 mM and 1 mM of dopamine. Saturation levels regarding the dopamine sensor was achieved at 14 μm and at 2.5 mM for the glutamate sensor. In both cases, no change in the amperometric signal obtained due to the presence of the interfering neurochemical is observed. Thus, these experiments demonstrate the selectivity of the developed sensor towards dopamine and glutamate by illustrating how the presence of concentration of one target is isolated from the measurement of the other target. Dopamine and glutamate concentration levels can therefore be measured by our system simultaneously.

For both glutamate and dopamine experimental detection, the lowest concentration values detected were limited by the noise generated by the experimental setup, especially caused by the rotation of the magnet in the magnetic beaker, and the wires used. In fact, before all injections of neurotransmitters, the current level recorded at the stabilization point of WE was about 1 nA due to thermal and mechanical noise. Therefore, in the case of the experimental results obtained for dopamine and glutamate measurements and depicted in Fig. 15, the wide dynamic range of our design could not be fully demonstrated due to these limitations. Although, as stressed in the introduction, a wide dynamic range is critical to measure a large variety of neurochemicals present in different concentration ranges in the brain

TABLE II
COMPARISON OF BIOSENSOR SYSTEMS FOR NEUROTRANSMITTERS DETECTION

	Transduction Mechanism	Tech (um)	Max. Sampling Frequency (Hz)	Current Range Detected	Channel Power (μW)	Sensitivity /Selectivity Considered	Experimental Multi-Neurotransmitter Detection
Li et al. [9]	Potentiometry (ISFET)	0.35	–	40 nA-6μA	–	No/Yes	No
Wang et al. [10]	Capacitive	0.35	0.03	–	–	No/Yes	No
Kim et al. [12]	Amperometry	0.5	2000	1-500 pA	–	No/No	No
Nazari et al. [13]	Amperometry/Voltammetry	0.35	1000	24 pA-300 nA	188	No/No	No
Mollazadeh et al. [14]	Amperometry	0.5	1000	100 pA-400nA	42	No/No	No
This Work	**Amperometry**	**0.13**	**4000**	**20 pA-600 nA**	**56**	**Yes/Yes**	**Yes**

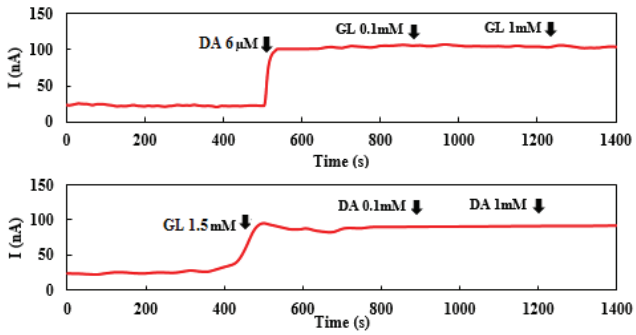

Fig. 17. Interference free detection of dopamine (top) and glutamate (bottom) dedicated sensors.

fluid, and the presented system is experimentally capable of this wide range concentration detection as shown by Fig. 14 curves. However, the fully-integrated solution proposed on Fig. 1 using wire-bounding connections, and the natural flow of the cerebral liquid circuling next to the electrode interface would allow picoamps detection. Moreover, concerning the potentiostat implementation, the final condition of the generated V_{ref} function may be adjusted according to the calibration curve associated to each detected neurotransmitter, in order to minimize power consumption and to increase the sampling frequency to its maximum of 4 kHz is necessary. Indeed, as mentioned previously, the amperometric response is determined by the physiological concentration of the neurochemical to be sensed and the applied functionalization of the corresponding WE. Thus, the detection of certain neurotransmitters only require nanoamps measurements to cover physiological concentrations, the picoamperes range detection becoming impertinent, allowing to increase the sampling frequency. Table II provides a comparison of different biosensor systems for neurotransmitters analysis, in terms of the application important specifications detailed in the introduction. The proposed system offers the best combination of sampling frequency, channel power and input current dynamic range. Moreover, the proposed system is the only one to consider sensitivity and selectivity issues. This work is also the only one to measure experimentally more than one neurochemical at a time. These results justify the pursue of this work towards an on-chip multi-electrode platform for a completely integrated sensor, as depicted on Fig. 1.

VI. CONCLUSION

Within the frame of a fully-integrated amperometric biosensor for multi-neurochemical detection, the design and experimental validation of its detection circuit and multi-target sensing platform was described. The proposed system consists of a time-based CMOS potentiostat optimized for neurotransmitters detection and a multiplexed WE platform functionalized with CNT-based composite films for selective and sensitive measurements of glutamate and dopamine. The fabricated potentiostat IC achieves a trade-off between a wide dynamic input range of 20 pA to 600 nA with a minimum and maximum sampling frequency of 1.25 kHz and 4 kHz, and a low power consumption of 56 μW. The overall functionality of the prototype detection system was verified by performing CA analysis of a dopamine and glutamate solution, at different concentration levels. Amperometric measurements results showed high selectivity and high linear response towards both neurotransmitters. This electrochemical system is the first to propose a solution for neurochemical detection that takes in account the molecular complexity of the *in vivo* environment and sensitivity issues related to miniaturization. This work demonstrates the feasibility of the proposed amperometric detection circuit, which could be extended to the detection of a wide variety of neurochemical using CNT-based customized sensors.

ACKNOWLEDGMENT

The authors are grateful for the design and simulation tools supplied by CMC Microsystems. Thanks are due to C. Boero for the microfabricated chip and her helpful advice.

REFERENCES

[1] M. Laruelle, L. S. Kegeles, and A. Abi-Dargham, "Glutamate, dopamine, and schizophrenia: From pathophysiology to treatment.," *Ann. NY Acad. Sci.*, pp. 138–158, Nov. 2003.
[2] D. L. Robinson, A. Hermans, A. T. Seipel, and R. M. Wightman, "Monitoring rapid chemical communication in the brain," *Chem. Rev.*, vol. 108, no. 7, pp. 2554–2584, 2008.
[3] M. Perry, Q. Li, and R. T. Kennedy, "Review of recent advances in analytical techniques for the determination of neurotransmitters," *Analytica. Chimica. Acta.*, vol. 653, no. 1, pp. 1–22, 2009.
[4] C. J. Watson, B. J. Venton, and R. T. Kennedy, "In vivo measurements of neurotransmitters by microdialysis sampling," *Anal. Chem.*, vol. 78, no. 5, pp. 1391–1399, 2006.
[5] P. M. Levine, P. Gong, R. Levicky, and K. L. Shepard, "Active CMOS sensor array for electrochemical biomolecular detection," *IEEE J. Solid-State Circuits*, vol. 43, no. 8, pp. 1859–1871, Aug. 2008.
[6] A. Manickam, A. Chevalier, M. McDermott, and A. D. Ellington, "A CMOS electrochemical impedance spectroscopy (EIS) biosensor array," *IEEE Trans. Biomed. Circuits Syst.*, vol. 4, no. 6, pp. 379–390, Dec. 2010.
[7] Z. Muhammad-Tahir and E. C. Alocilja, "Fabrication of a disposable biosensor for Escherichia Coli O157:H7 detection," *IEEE Sensors J.*, vol. 3, no. 4, pp. 345–351, Aug. 2003.
[8] C. Yang, H. Yue, B. L. Hassler, R. M. Worden, and A. J. Mason, "Amperometric electrochemical microsystem for a miniaturized protein biosensor array," *IEEE Trans. Biomed. Circuits Syst.*, vol. 3, no. 3, pp. 160–168, June 2009.

[9] D.-C. Li, P.-H. Yang, and M. S.-C. Lu, "CMOS open-gate ion-sensitive field effect transistors for ultrasensitive dopamine detection," *IEEE Trans. Electron Devices*, vol. 57, no. 10, pp. 2761–2767, 2010.

[10] S.-W. Wang and M. S.-C. Lu, "CMOS capacitive sensors with sub-μm microelectrodes for biosensing applications," *IEEE Sensors J.*, vol. 10, no. 5, pp. 991–996, 2010.

[11] C. Lei-Guang and M. S.-C. Lu, "Glass-based integrated capacitive sensors for detection of the neurotransmitter dopamine," *IET Micro Nano Lett.*, vol. 6, no. 7, pp. 482–485, 2011.

[12] B. N. Kim, A. D. Herbst, S. J. Kim, B. A. Minch, and M. Lindau, "Parallel recording of neurotransmitters release from chromaffin cells using a 1010 CMOS IC potentiostat array with on-chip working electrodes," *Biosens. Bioelectron.*, vol. 41, pp. 736–744, 2013.

[13] M. H. Nazari, H. Mazhab-Jafari, L. Leng, A. Guenther, and R. Genov, "CMOS neurotransmitter microarray: 96-channel integrated potentiostat with on-die microsensors," *IEEE Trans. Biomed. Circuits Syst.*, vol. 7, no. 3, pp. 338–348, 2013.

[14] M. Mollazadeh, K. Murari, G. Cauwenberghs, and N. V. Thakor, "Wireless micropower instrumentation for multimodal acquisition of electrical and chemical neural activity," *IEEE Trans. Biomed. Circuits Syst.*, vol. 3, no. 6, pp. 388–439, 2009.

[15] A. J. Bard and L. R. Faulkner, *Electrochemical Methods: Fundamentals and Applications*, 2nd ed. Hoboken, NJ, USA: Wiley, 2000.

[16] D. S. Robertson, "The physical chemistry of brain and neural cell membranes: An overview," *Neurochem. Res.*, vol. 35, no. 5, pp. 681–687, 2010.

[17] E. Kandel, J. Schwartz, and T. Jessell, "Principles of Neural Science," in *Principles of Neural Science*, 5th ed. New York, NY, USA: McGraw-Hill Education, 2013.

[18] D. Robert, R. O'Neill, P. Lowry, and M. Manuel, "Monitoring brain chemistry in vivo: Voltammetric techniques, sensors, and behavioral applications," *Crit. Rev. Trade Neurobiol.*, vol. 12, no. 1–2, pp. 69–127, 1998.

[19] D. J. Michael and R. M. Wightman, "Electrochemical monitoring of biogenic amine neurotransmission in real time," *J. Pharm. Biomed. Anal.*, vol. 19, no. 1–2, pp. 33–46, 1999.

[20] W. P. Kang, S. Raina, J. L. Davidson, and H. H. Huang, "Temporal resolution electrochemical biosensor using nitrogen-incorporated nanodiamond ultra-microelectrode array," in *Proc. IEEE Sensors Conf.*, 2012, vol. 28–31, no. 1–2, pp. 1489–1492.

[21] M. Stanacevic, K. Murari, A. Rege, G. Cauwenberghs, and N. V. Thakor, "VLSI potentiostat array with oversampling gain modulation for wide-range neurotransmitter sensing," *IEEE Trans. Biomed. Circuits Syst.*, vol. 1, no. 1, pp. 63–72, 2007.

[22] K. Murari, N. V. Thakor, M. Stanacevic, and G. Cauwenberghs, "Wide-range, picoampere-sensitivity multichannel VLSI potentiostat for neurotransmitter sensing," in *Proc. 26th Annu. Int. Conf. Engineering in Medicine and Biology Soc.*, 2004, vol. 2, pp. 4063–4066.

[23] R. Genov, M. Stanacevic, M. Naware, G. Cauwenberghs, and N. Thakor, "16-channel integrated potentiostat for distributed neurochemical sensing," *IEEE Trans. Circuits Syst. I, Reg. Papers*, vol. 53, no. 11, pp. 2371–2376, Nov. 2006.

[24] M. Breten, T. Lehmann, and E. Braun, "Integrating data converters for picoampere currents from electrochemical transducers," in *Proc. IEEE Int. Symp. Circuits and Systems*, Geneva, Switzerland, 2000, vol. 5, pp. 709–712.

[25] H. S. Narula and J. G. Harris, "A time-based VLSI potentiostat for ion current measurements," *IEEE Sensors J.*, vol. 6, no. 2, pp. 239–247, 2006.

[26] C. B. Jacobs, M. J. Peairs, and B. J. Venton, "Review: Carbon nanotube based electrochemical sensors for biomolecules," *Analytica Chimica. Acta.*, vol. 662, no. 2, pp. 105–127, 2010.

[27] J. Wang, "Carbon-nanotube based electrochemical biosensors: A review," *Electroanalysis.*, vol. 17, no. 1, pp. 7–14, 2005.

[28] L. Ag, P. Yez-Sedeo, and J. M. Pingarrn, "Role of carbon nanotubes in electroanalytical chemistry: A review," *Analytica Chimica. Acta.*, vol. 622, no. 1–2, pp. 11–47, 2008.

[29] D. A. X. Nayagam, R. A. Williams, J. Chen, K. A. Magee, J. Irwin, J. Tan, P. Innis, R. T. Leung, S. Finch, C. E. Williams, G. M. Clark, and G. G. Wallace, "Carbon nanotubes: Biocompatibility of immobilized aligned carbon nanotubes," *Small J.*, vol. 7, no. 8, pp. 1035–1042, 2011.

[30] W. Feng and P. Ji, "Enzymes immobilized on carbon nanotubes," *Biotechnol. Adv.*, 2011.

[31] R. N. Goyal and S. Bishnoi, "Simultaneous determination of epinephrine and norepinephrine in human blood plasma and urine samples using nanotubes modified edge plane pyrolytic graphite electrode," *Talanta*, vol. 84, pp. 78–83, 2011.

[32] M. A. Kamyabi, O. Narimani, and H. H. Monfared, "Electroless deposition of bis(4'-(4-Pyridyl)-2,2':6', 2"-terpyridine)iron(II) thiocyanate complex onto carbon nanotubes modified glassy carbon electrode: Application to simultaneous determination of ascorbic acid, dopamine and uric acid," *J. Brazil Chem. Soc.*, vol. 22, pp. 468–477, 2011.

[33] A. Abbaspour and A. Noori, "A cyclodextrin host-guest recognition approach to an electrochemical sensor for simultaneous quantification of serotonin and dopamine," *Biosens. Bioelectron.*, vol. 26, pp. 4674–4680, 2011.

[34] P. M. Figueiredo and J. C. Vital, "Low kickback noise techniques for CMOS latched comparators," in *Proc. Int. Symp. Circuits and Systems*, 2004, vol. 1, pp. I-537–I-540.

[35] S.-C. Yi, "A 6-bit digital to analogue converter based on current mirrors," *Int. J. Electron.*, vol. 99, no. 9, pp. 1291–1298, 2012.

[36] C. C. Enz, F. Krummenacher, and E. Vittoz, "An analytical MOS transistor model valid in all regions of operation and dedicated to low-voltage and low-current applications," *Analog Integrated Circuits Signal Process.*, vol. 8, pp. 83–114, 1995.

[37] C. Boero, J. Olivo, G. De Micheli, and S. Carrara, "New approaches for carbon nanotubes-based biosensors and their application to cell culture monitoring," *IEEE Trans. Biomed. Circuits Syst.*, vol. 6, no. 5, pp. 479–485, 2010.

[38] I. J. Wang, M. Musameh, and Y. Lin, "Solubilization of carbon nanotubes by naon toward the preparation of amperometric biosensors," *J. Amer. Chem. Soc.*, vol. 125, no. 9, pp. 2408–2409, 2003.

[39] S. Chakraborty and C. Retna Raj, "Amperometric biosensing of glutamate using carbon nanotube based electrode," *Electrochem. Commun.*, vol. 9, pp. 1323–1330, 2009.